Supporting Information for:

Novel porous polymorphs of zinc cyanide with rich thermal and mechanical behavior

Fabien Trousselet,[1] Anne Boutin,[1,*] and François-Xavier Coudert[2,†]

[1] *École Normale Supérieure, PSL Research University, Département de Chimie, Sorbonne Universités – UPMC Univ Paris 06, CNRS UMR 8640 PASTEUR, 24 rue Lhomond, 75005 Paris, France*

[2] *PSL Research University, Chimie ParisTech – CNRS, Institut de Recherche de Chimie Paris, 75005 Paris, France*

Complement to Section V.A

The distributions of radial distances $g(r_{\mathrm{Zn-C/N}})$, shown in Fig. S5, allow to distinguish different types of transitions. For either dense or porous structures, the first two peaks (labeled 1 and 2 on the Figure, at $\simeq$ 2 and $\simeq$ 3.1 Å respectively) are associated to the cyanide ions coordinating the zinc, and show very little evolution under pressure. For the *dia-c* structure, a third (very broad) peak at distances $r \leq 5.0$ Å is also visible; it corresponds to the distances between a given Zn, in one of the interpenetrated *dia* frameworks, and the nearest cyanide ions from the other framework. With increasing pressure, this peak shifts significantly to shorter distances (from 4.9 at zero pressure to 4.4 Å at $P = 2.0$ GPa) and simultaneously broadens. This shift is reminiscent of the experimental observation by Collings et al. that, in the high-pressure phase of $Zn(CN)_2$, the corresponding distances (shown in Fig. 9 of Ref.1) decrease with increasing pressure, with a tendency towards 6-fold coordination of Zn at very large pressures. Our approach fails to describe reliably the high-pressure phase, but we suspect that both features are indeed connected and propose the following mechanism: an increase in pressure tends to amplify the *buckling vibrations* (or $\langle\theta^2\rangle$) of a cyanide ion around its Zn–Zn axis. While such vibrations have little impact on the positions of peaks 1 and 2 in $g_{\mathrm{Zn-C/N}}(r)$ (at order 2 only in θ), they impact much more the distances corresponding to the 3rd peak (at order 1 in θ), accounting for its broadening and shift towards smaller distances. The latter shift is favored by (a combined effect of van der Waals interactions and) compression. The distributions of Zn–C/N radial distances r' evaluated on time-averaged atomic positions — see Fig. S5(c) where the third peak seems is converted for $P > 1.2$ GPa into a very broad feature — indicate that this transition is accompanied by a substantial increase of disorder in the relative atomic positions of distinct frameworks.

This effect should also happen in the *mok* phase where $g_r(\mathrm{Zn–C/N})$ presents also a broad peak, of similar nature, around 5 Å, but not in the porous phases where such a peak is absent (see Fig. S5-(a)). This may explain the fact that pressure-induced transitions are of different nature in porous structures (at lower pressures, and with a clear discontinuity in volume). The suspected driving mechanism for these transitions is rather a mode softening, that can be evidenced by the evolution of elastic constants.

* Email: anne.boutin@ens.fr
† Email: fx.coudert@chimie-paristech.fr. Twitter: @fxcoudert. Web: http://coudert.name/
1 I. Collings et al., *J. Am. Chem. Soc.* **135**, 7610(2013).

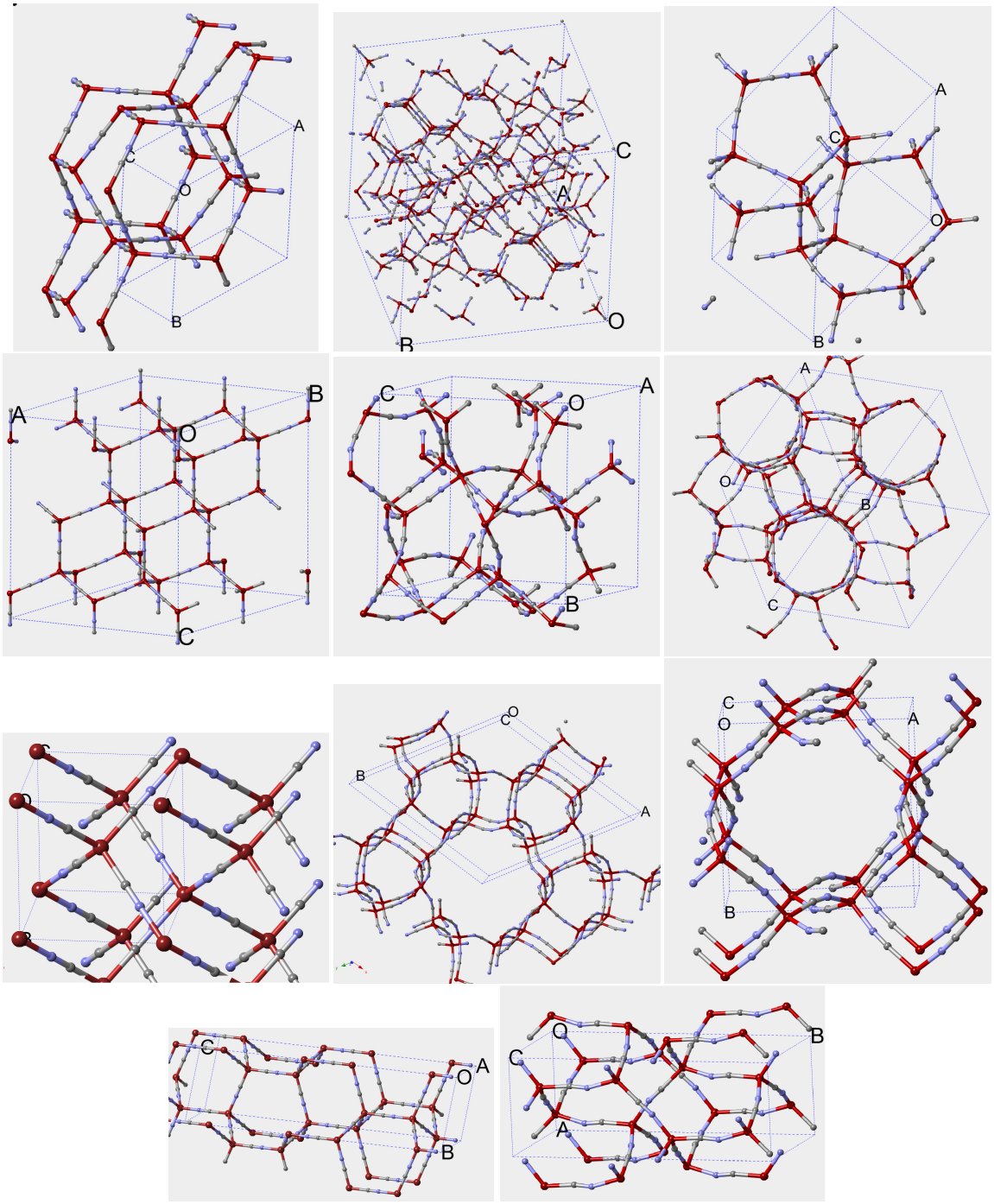

Figure S1. The eleven T= 0K structures of $Zn(CN)_2$ studied in this work, as obtained from energy-minimzation. Unit cells are indicated, and a bit more than 1 unit cell is shown to better give account of the structure's topology. Color code: Zn in red, C in grey, N in blue. Top line, from left to right: *lon*, *che*, *unj*; Second line: *dia*, *gsi*, *lcs*; Third line: *dia-c*, *una*, *unc*; Last line: *cfc*, *mok*.

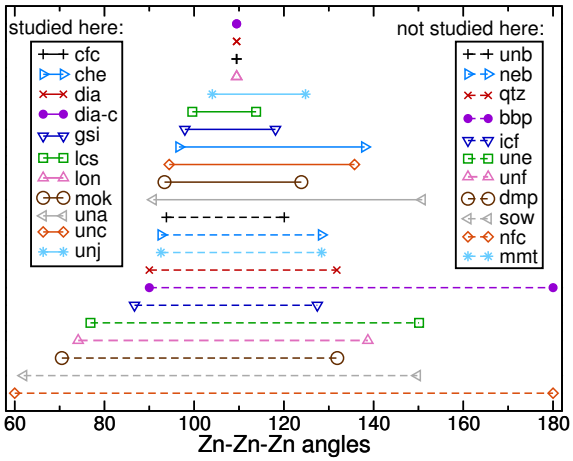

Figure S2. Minimal and maximal values of Zn–Zn–Zn angles in (i) the nets considered in this study (11 uppermost points/continuous lines) and (ii) other 4-coordinated nets found in the RCSR database, but not considered in the study.

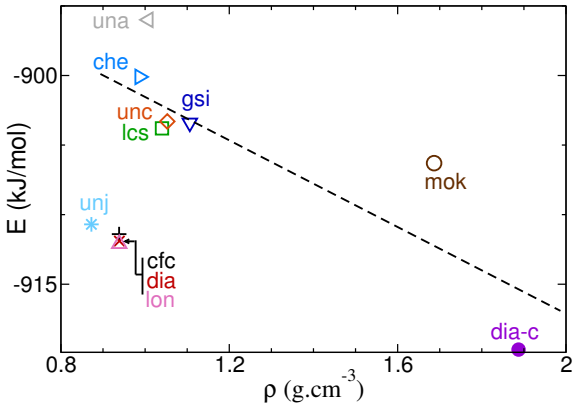

Figure S3. Energy of zinc cyanide polymorphs (per $Zn(CN)_2$ unit) versus density. For each polymorph, the structure was obtained by re-optimizing, with the MD force field (and near-zero Kelvin dynamics), the corresponding structure found by DFT.

Framework	α_a	α_b	α_c	α_V
cfc	-12.62	-12.74	-12.58	-37.94
che	-13.50	-13.54	-13.37	-40.41
dia	-13.13	-13.15	-12.65	-38.93
dia-c	-11.86	-12.18	-11.82	-35.86
gsi	-13.28	-13.31	-13.54	-40.13
lcs	-14.90	-14.90	-14.82	-44.62

Framework	α_a	α_b	α_c	α_V
lon	-12.92	-12.79	-12.68	-38.39
mok	-8.29	14.01	-5.71	0.01
una	-13.70	-13.60	-14.28	-41.58
unc	-14.36	-14.20	-14.93	-43.49
unj	-12.21	-12.22	-11.72	-36.15

Table S1. Table giving, for each $Zn(CN)_2$ framework listed, the linear thermal expansion coefficients $\alpha_i = \frac{1}{l_i}\left(\frac{dl_i}{dT}\right)$, with $l_i = a, b, c$ the cell parameters; additionally the volume thermal expansion coefficient $\alpha_V = \frac{1}{V}\left(\frac{dV}{dT}\right)$ is also given. Values are in MK^{-1}. Note that, apart from the *mok* case, for a given framework the 3 linear expansion coefficients differ from each other by 5 percent at most.

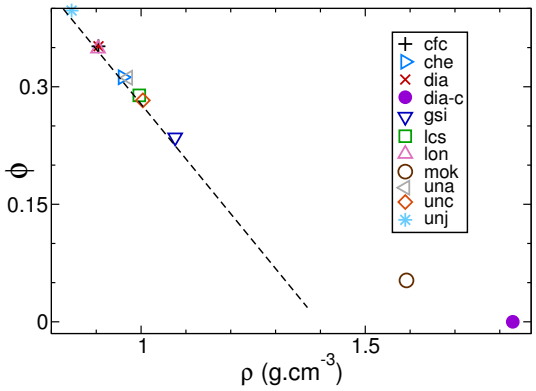

Figure S4. Porosity ϕ as a function of density ρ for the structures listed, at T = 0 K and P = 0.

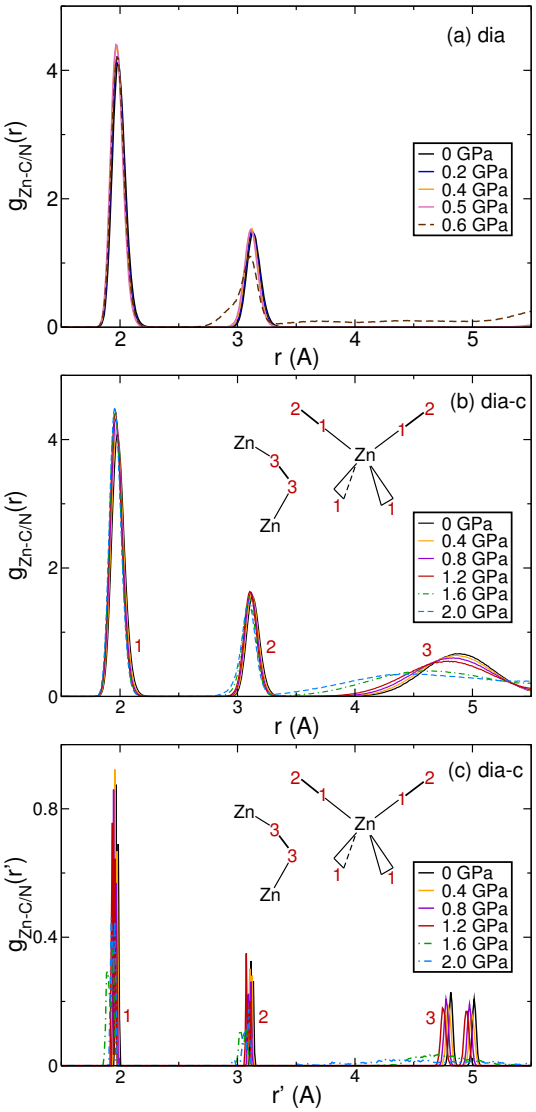

Figure S5. Distributions of Zn-X distances r (in ångströms) between a Zn atom and other types of atoms (X=C or N), for the *dia* (a) and *dia-c* (b) structures, at T = 300 K and pressures P indicated in the legend. For the *dia-c*, peaks refer to the type of C/N atoms, as indicated in the cartoon (1: nearest atom of a cyanide coordinating the Zn atom; 2: other atom of such a cyanide; 3: atoms of a further neighbor cyanide, not coordinating this Zn).(c): distributions of distances r' of the same type as in (b), but evaluated on time-averaged structures.

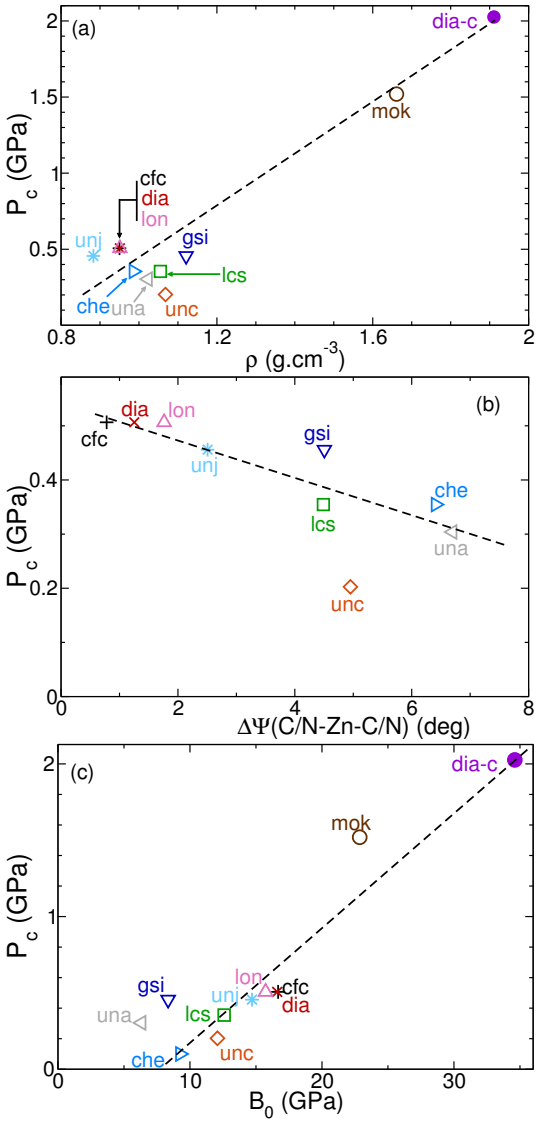

Figure S6. Plots showing the critical pressure P_c (in GPa, estimated from MD simulations at T= 300 K) versus (a) the framework density (estimated in MD at the same temperature and zero pressure); (b) the root mean square deviation ΔΨ of C/N–Zn–C/N angles (in degrees, estimated from T = 0 K structures); or (c) the bulk modulus B_0 at (in GPa, estimated from MD simulations at T= 300 K).

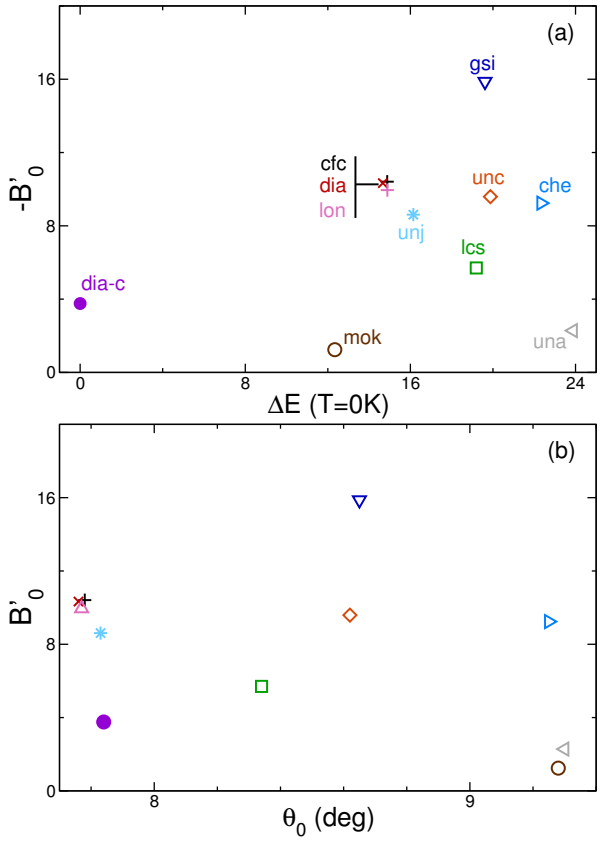

Figure S7. Coefficients B_o' estimated from MD simulations at T = 300K and subsequent fits to Eq. (4) in the paper, for the 11 structures indicated; they are plotted against (a) the DFT-obtained energy $\Delta E(T = 0K)$ (in kJ/mol); and (b) the angle θ_o (in degrees).

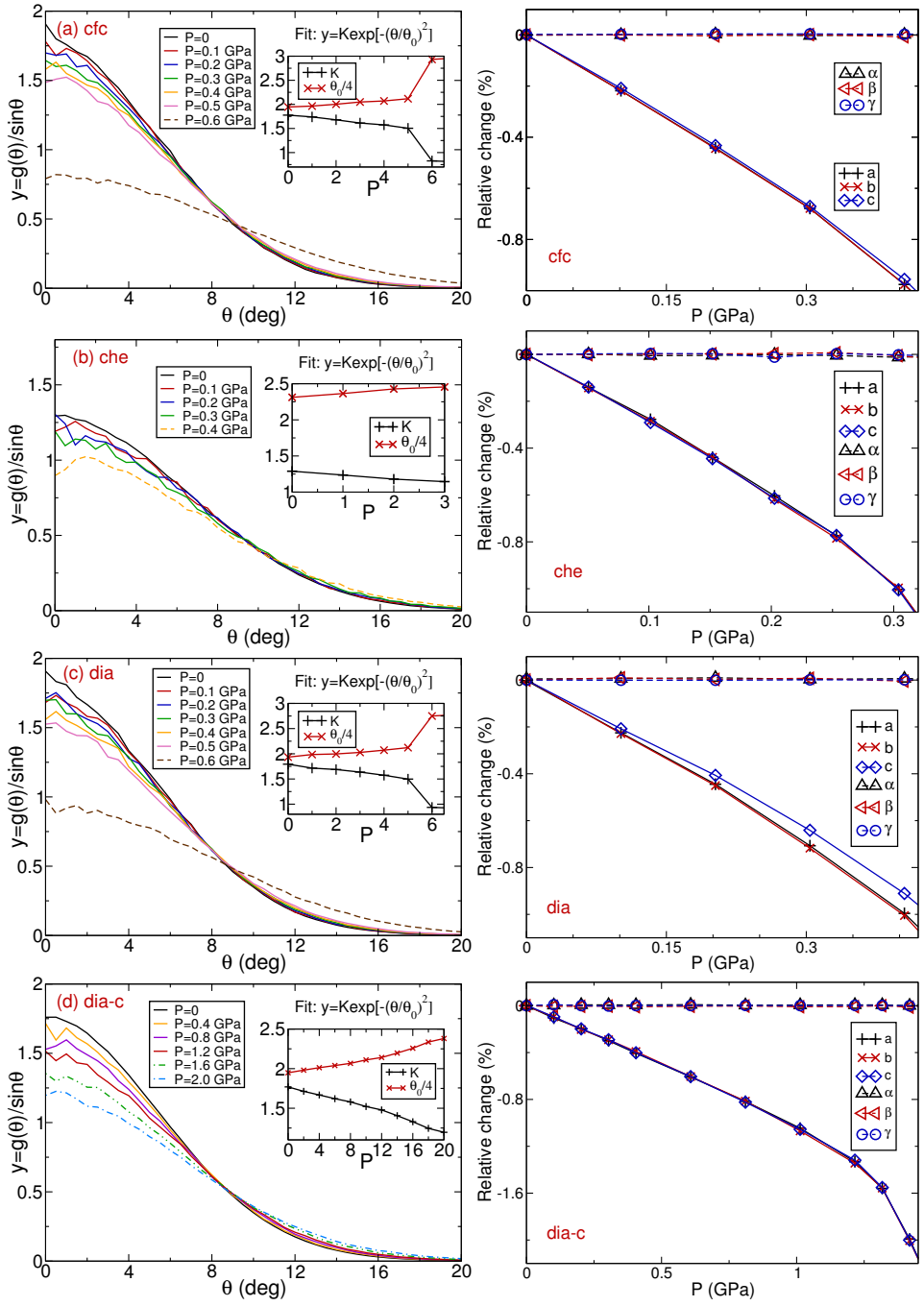

Figure S8. Evolution of structures (a) *cfc*, (b) *che*, (c) *dia*, and (d) *dia-c* under pressure, at T = 300 K (in MD simulations of stepwise compression). Left: functions $g(\theta)/\sin(\theta)$ with $g(\theta)$ the distribution of angle θ (see inset in Fig. 4 of the main text) at pressures indicated in the captions. Right: Relative evolution of cell parameters a, b, c and cell angles α, β, γ versus pressure.

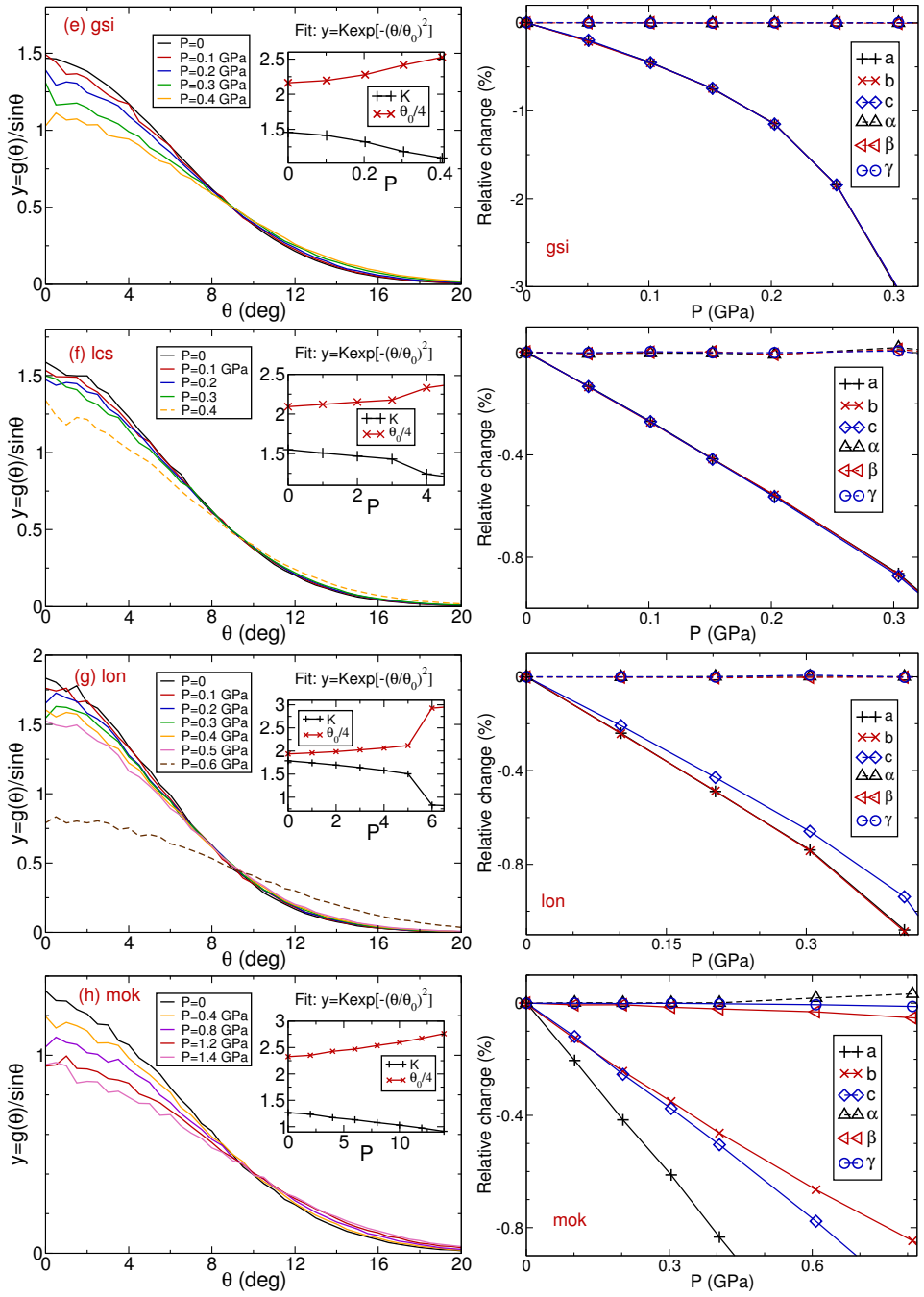

Figure S9. Similar content as in Fig. S8, but for the following structures: (e) *gsi*, (f) *lcs*, (g) *lon*, and (h) *mok*.

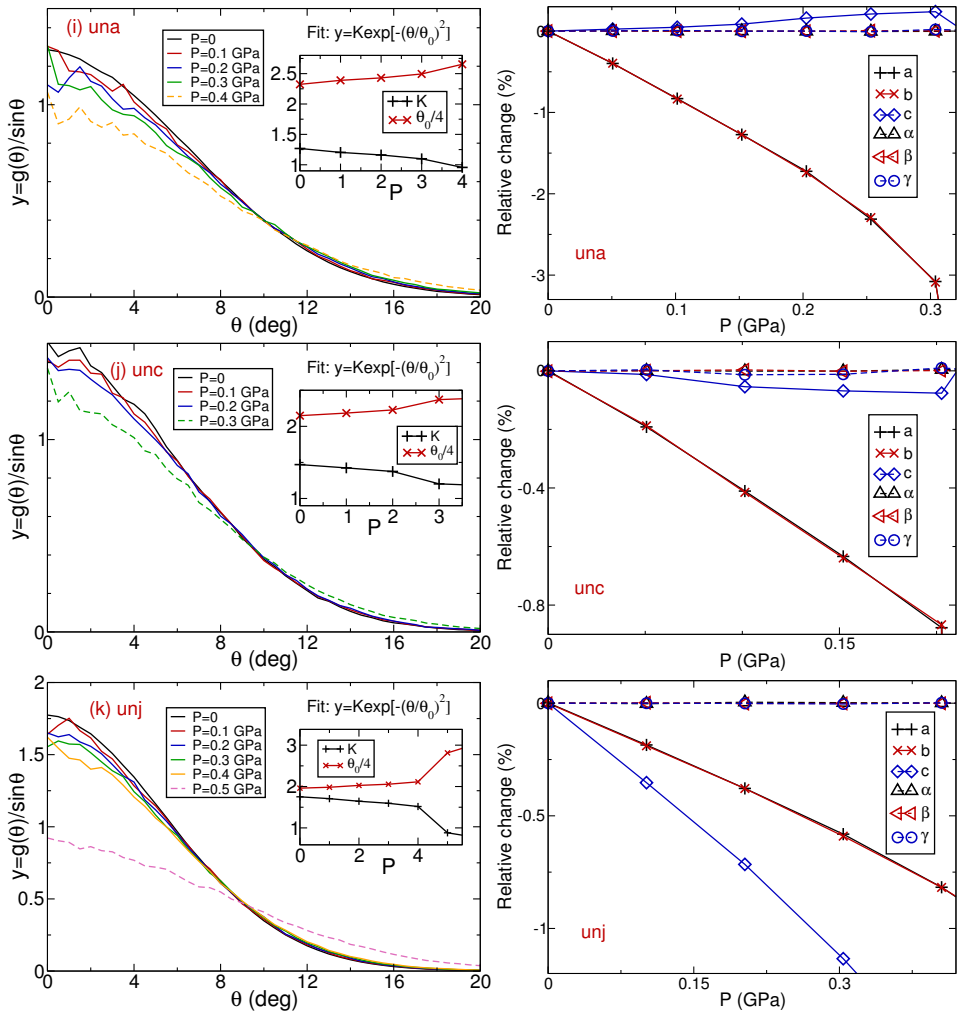

Figure S10. Similar content as in Fig. S8, but for the following structures: (i) *una*, (j) *unc*, and (k) *unj*.